DISCRETE MACROSCOPIC TRAFFIC FLOW MODEL CONSIDERING LANE-CHANGING BEHAVIORS IN THE MIXED TRAFFIC ENVIRONMENT

Yi Zhang
Ph.D. Student & Graduate Research Assistant
Department of Civil and Environmental Engineering
University of Maryland, College Park, MD, U.S., 20742
Email: zhangyi@umd.edu

Kaitai Yang
Ph.D. Student & Graduate Research Assistant
Department of Civil and Environmental Engineering
University of Maryland, College Park, MD, U.S., 20742
Email: kaitai74@umd.edu

Yuanzheng Lei
Ph.D. Student & Graduate Research Assistant
Department of Civil and Environmental Engineering
University of Maryland, College Park, MD, U.S., 20742
Email: yzlei@umd.edu

Yaobang Gong, Ph.D.
Postdoctoral Research Associate
Department of Civil and Environmental Engineering
University of Maryland, College Park, MD, U.S., 20742
Email: ybgong@umd.edu

Xianfeng (Terry) Yang, Ph.D.
Assistant Professor
Department of Civil and Environmental Engineering
University of Maryland, College Park, MD, U.S., 20742
Email: xtyang@umd.edu

Word Count: 6544 words + 3 table (250 words per table) = 7,294 words

Submitted August 1st, 2023.

ABSTRACT

In the foreseeable future, the coexistence of connected automated vehicles (CAVs) and human-driven vehicles (HVs) will persist in the traffic landscape for an extended duration. The accurate estimation of the mixed traffic status becomes crucial to effectively manage traffic flow and ensure road safety. In this research, we introduce a discrete macroscopic second-order traffic flow model tailored to capture the intricacies of the mixed traffic environment. Building upon a microscopic traffic model, our proposed approach considers the interactions between CAVs and HVs, as well as the distinctive driving behaviors exhibited by each vehicle type. Notably, we conduct an in-depth analysis of car-following and lane-changing behaviors observed in human-driven vehicles. To assess the efficacy of our proposed model, we conducted extensive numerical simulations on a freeway segment involving speed control. The results of the simulations reveal two key findings: Firstly, the proposed model achieves accurate estimations of mixed traffic states, encompassing both flow and speed parameters. Secondly, we observe a noteworthy enhancement in performance as the speed control disparity between CAVs and HVs increases. Our research contributes to advancing traffic management strategies and paves the way for enhanced traffic flow in mixed traffic environments. Furthermore, the proposed model holds significant potential for aiding the design and implementation of future transportation systems that embrace connected automated vehicles while accommodating human-driven vehicles seamlessly.

Keywords: Macroscopic Traffic Model, Lane-changing Behavior, Mixed Traffic Flow, CAV

INTRODUCTION

Through the exchange of real-time information between vehicles and infrastructures, applications involving Connected and Automated Vehicles (CAVs) have exhibited promising advantages in enhancing transportation safety (*1*) and mobility(*2*). CAV technology has demonstrated significant potential in addressing traffic congestion and enhancing the efficiency of transportation systems(*3*, *4*). Aiming to explore potential benefits, many researchers have conducted investigations into the applications of CAV technology across various traffic control domains(*5*–*7*). Such endeavors aid traffic agencies in deploying CAV applications effectively in the real world.

However, due to the constraints in technical development, it is foreseeable that CAVs will need to coexist with human-driven vehicles (HVs) and share the road network in the recent future. For the control of CAVs in the mixed traffic environment, it is important to propose a traffic estimation model, which can capture the mixed CAV and HV traffic pattern, to support traffic operation research and applications(*8*–*12*). Nevertheless, the conventional macroscopic traffic state model fails to encapsulate the influence of controlled CAVs on the overall freeway traffic state in most CAV applications.

Despite the abundance of literature on mixed traffic environments comprising both CAVs and human-driven vehicles HVs (*13*–*15*), the current models mainly focused on the fundamental diagram(*15*–*21*) and there remains a significant gap in fully capturing the intricate interactions between these vehicle types. Existing studies have not adequately addressed crucial aspects such as CAVs operating under dynamic trajectory control with varying speeds, which directly impact the behavior of following HVs in the traffic stream. Additionally, the link between sharp vehicle speed reductions and the triggering of lane-changing behavior in following vehicles has not been thoroughly investigated, despite its potential impact on the overall traffic pattern. The research gap is threefold: Firstly, there is a need to develop a macroscopic traffic flow model that accurately incorporates the lane-changing and car-following behaviors of HVs, thus enabling a comprehensive representation of the interactions between CAVs and HVs. Secondly, current models lack mechanisms to effectively handle variable speed limit control for both CAVs and HVs in mixed traffic environments, despite its importance in optimizing traffic flow. Lastly, the impact of factors such as the penetration rate of CAVs and the compliant rate of drivers on freeway traffic dynamics requires further exploration to better understand their role in shaping the overall traffic behavior in a mixed traffic scenario. Addressing these critical issues will significantly advance our understanding of mixed traffic dynamics and pave the way for more efficient and safe transportation systems that seamlessly integrate CAVs and HVs.

This study aims to tackle the aforementioned challenges by proposing a novel second-order multi-class macroscopic traffic state model that effectively captures the complex interactions between CAVs and HVs as distinct groups. By conducting a comprehensive kinematic analysis of both vehicle types, the proposed macroscopic model emerges, overcoming the limitations of existing approaches. In this research, we derive the macroscopic traffic model from a microscopic counterpart, incorporating essential features such as HV drivers' lane-changing behavior and their response to variable speed limit (VSL) control. This integration of lane-changing dynamics and VSL response enhances the model's realism and provides a more accurate representation of real-world mixed traffic scenarios. By explicitly differentiating CAVs and HVs in the model, we gain deeper insights into their unique driving characteristics and their influence on overall traffic dynamics. The model's multi-class nature allows us to study the distinct behavioral patterns exhibited by CAVs and HVs separately, providing a comprehensive understanding of their interactions and impact on traffic flow.

The following sections of this paper are structured as: Section 2 presents the methodology based on kinematic analysis and mathematics modeling. Section 3 describes the design of the numerical

experiment, followed by the discussion on the effectiveness of the traffic model proposed in this research in Section 4. Lastly, the conclusion is presented in the final section.

METHODOLOGY

In this section, the mathematical model is proposed based on the analysis of different kinds of vehicles to estimate the traffic status of mixed traffic environment with variable speed limit (VSL) that was guided by roadside unit (for CAVs) and changeable message signs (for HVs). Traffic sensors located at the roadside that could gather traffic flow status, such as speed, and flow rate, could be used as the input of the model.

In a mixed traffic environment, two types of vehicles coexist: CAVs and HVs. CAVs, controlled by a central system, strictly adhere to the VSL and only change lanes when necessary. On the other hand, HVs, controlled by individual drivers, may or may not follow the speed limit instructions. Compliant human drivers adjust their speed to match the VSL. When the leading vehicle decreases its speed due to the VSL, these compliant drivers also reduce their vehicle speed and continue to follow the leading vehicle. However, some drivers may choose not to comply with the displayed speed limit information. In such cases, when the leading vehicle decreases its speed, these non-compliant drivers might change lanes to maintain a higher speed. To build the model for a general mixed traffic flow environment, the following assumptions are considered:

1. The road geometry will not affect the driver's behavior and vehicle movement.
2. The weather condition is assumed to be fine and will not affect the driver's behaviors and vehicle movements.
3. Drivers will not change their lanes randomly, lane-changing decisions are induced by variable speed limits.
4. The driver's characteristics and personalities are the same and will not affect the driver's behavior and vehicle movement.
5. Different vehicles (CAV, Compliant HV, Uncompliant HV, Lane-changing HV) are evenly distributed on the road.
6. Vehicles of the same type have the same movement criteria and will not affect the driver's behavior and vehicle movement.
7. The human drivers are greedy, if the lane-changing conditions are satisfied, they will change the lane.

In this research, the authors are aiming at proposing a discrete macroscopic traffic flow model in a mixed traffic environment to predict the traffic status for the following time interval. The vehicle behaviors including car-following and lane-changing are considered separately in microscopic scope to build the model in macroscopic scope.

Vehicle Moving Analysis

Vehicle Type 1: CAV

In microscopic, CAVs are assumed to keep following the previous vehicle and are controlled by the control center. The car-following behavior of CAV could be described as(*22*):

$$\dot{v}_i(t) = \frac{V^{CAV}\left(\dot{s}_i(t)\right) - v_i(t)}{\tau} - \gamma\left(v_i(t) - v_{i+1}(t)\right) \quad (1.)$$

where, $\dot{v}_i(t)$ is the acceleration function of vehicle i over time; $V^{CAV}\left(\dot{s}_i(t)\right)$ is the optimal velocity function of CAV; $v_i(t)$ is the current speed of CAV; $v_{i+1}(t)$ is the current speed of the previous vehicle; τ represents sensitivity for speed differences between current speed and optimal velocity of CAV; and γ represents the sensitivity for speed differences between current speed and leading vehicle's speed.

The acceleration of CAV is related to the optimal velocity from the control center and the speed difference between CAV and the leading vehicle. The speed function over time could be formulated by integration as:

$$v_i(t) = v_i(t_0) + \int_{t_0}^{t_0+\Delta T} \left(\frac{V^{CAV}\left(\dot{s}_i(t)\right) - v_i(t)}{\tau} - \gamma\left(v_i(t) - v_{i+1}(t)\right) \right) dt \qquad (2.)$$

From the microscopic to the macroscopic, the discrete macroscopic traffic flow model(*23*) for CAVs in road segment i and lane j at time interval $k+1$ could be written as:

$$v_{i,j}^{CAV}(k+1) = v_{i,j}^{CAV}(k) + \frac{\Delta T}{\tau_i}\left[V_{i,j}^{CAV}\left(d_{i,j}^{ALL}(k)\right) - v_{i,j}^{CAV}(k)\right] + \frac{\Delta T}{L_i} v_{i,j}^{CAV}(k)\left[v_{i-1,j}^{CAV}(k) - v_{i,j}^{CAV}(k)\right] - \frac{\nu_i \Delta T}{\tau_i L_i} \frac{\left[d_{i+1,j}^{ALL}(k) - d_{i,j}^{ALL}(k)\right]}{\left[d_{i,j}^{ALL}(k)\right]} \qquad (3.)$$

The optimal velocity function of CAV is related to $v_{f,i,j}^{CAV}$, which is the expected speed of CAV from the control center.

$$V_{i,j}^{CAV}\left[d_{i,j}^{ALL}(k)\right] = v_{f,i,j}^{VSL} \exp\left[-\frac{1}{a_{i,j}^{CAV}} \left(\frac{d_{i,j}^{ALL}(k)}{d_{cr,i,j}^{CAV}} \right)^{a_{i,j}^{CAV}} \right] \qquad (4.)$$

where:

$v_{i,j}^{CAV}(k+1)$ is the traffic speed of CAV on segment i and lane j at time $k+1$

$v_{i,j}^{CAV}(k)$ is the traffic speed of CAV on segment i and lane j at time k

$v_{i-1,j}^{CAV}(k)$ is the traffic speed of CAV on segment $i-1$ and lane j at time k

ΔT is the length of update time interval

L_i is the length of segment i

τ_i, ν_i, κ_i are the parameters in the dynamic speed equations of segment i

$V_{i,j}^{CAV}\left[d_{i,j}^{ALL}(k)\right]$ is the static speed of CAVs for segment i and lane j at time k with respect to the density of segment i and lane j at time k

$d_{i,j}^{ALL}(k)$ is the traffic density on road segment i and lane j at time interval k

$d_{cr,i,j}^{CAV}$ is the critical density for CAV on road segment i and lane j

$a_{i,j}^{CAV}$ is the speed exponent term of segment i and lane j for CAV

$v_{f,i,j}^{CAV}$, is the expected speed of CAV from the control center.

Vehicle Type 2: Compliant HV

The compliant HV will follow the VSL control instructions on the information board. Similarly, the car-following behavior of CHV based on FVDM and the speed function over time could be written as:

$$\dot{v}_i(t) = \frac{V^{CHV}\left(\dot{s}_i(t)\right) - v_i(t)}{\tau} - \gamma\left(v_i(t) - v_{i+1}(t)\right) \quad (5.)$$

where,

$\dot{v}_i(t)$ the acceleration function of vehicle i over time.

$V^{CHV}\left(\dot{s}_i(t)\right)$ the optimal velocity function of CHV

$v_i(t)$ the current speed of HV

$v_{i+1}(t)$ the current speed of the previous vehicle

τ sensitivity for speed differences between current speed and optimal velocity of HV

γ sensitivity for speed differences between current speed and leading vehicle's speed

$$v_i(t) = v_i(t_0) + \int_{t_0}^{t_0+\Delta T}\left(\frac{V^{CHV}\left(\dot{s}_i(t)\right) - v_i(t)}{\tau} - \gamma\left(v_i(t) - v_{i+1}(t)\right)\right)dt \quad (6.)$$

The macroscopic discrete velocity function of car-following CHVs in road segment i and lane j at time interval $k+1$ could be derivatized. The optimal velocity function of CHV is related to $v_{f,i,j}^{CHV}$, which is the driver's expected speed of HV. When there is no speed limitation, the CHV will drive with free-flow speed $v_{f,i,j}^{free}$ as the expected speed; when the CHV passes a speed limit spot, the expected speed of CHV $v_{f,i,j}^{CHV}$ will be the VSL speed $v_{f,i,j}^{VSL}$ because the CHV drivers will completely follow the speed limitation.

$$v_{i,j}^{CHV}(k+1) = v_{i,j}^{CHV}(k) + \frac{\Delta T}{\tau_i}\left[V_{i,j}^{CHV}\left(d_{i,j}^{ALL}(k)\right) - v_{i,j}^{CHV}(k)\right] + \frac{\Delta T}{L_i}v_{i,j}^{CHV}(k)\left[v_{i-1,j}^{CHV}(k) - v_{i,j}^{CHV}(k)\right] - \frac{v_i\Delta T}{\tau_i L_i}\frac{\left[d_{i+1,j}^{ALL}(k) - d_{i,j}^{ALL}(k)\right]}{\left[d_{i,j}^{ALL}(k)\right]} \quad (7.)$$

$$V_{i,j}^{CHV}\left[d_{i,j}^{ALL}(k)\right] = v_{f,i,j}^{CHV}\exp\left[-\frac{1}{a_{i,j}^{HV}}\left(\frac{d_{i,j}^{ALL}(k)}{d_{cr,i,j}^{HV}}\right)^{a_{i,j}^{HV}}\right] \quad (8.)$$

$$v_{f,i,j}^{CHV} = \begin{cases} v_{f,i,j}^{VSL}\ Under\ Control \\ v_{f,i,j}^{free}\ Otherwise \end{cases} \quad (9.)$$

Vehicle Type 3: Uncompliant HV

The uncompliant HV is proposed to describe the car-following behavior of those drivers who will not follow the speed limitation. For those vehicles, their desired speed will always be the free-flow speed no matter if they pass a speed control board. The UHV drivers prefer to drive at a higher speed rather than decrease their speed. The microscopic car-following behavior and speed integration function could be formulated by FVDM as follows:

$$\dot{v}_i(t) = \frac{V^{UHV}\left(\dot{s}_i(t)\right) - v_i(t)}{\tau} - \gamma\left(v_i(t) - v_{i+1}(t)\right) \quad (10.)$$

$$v_i(t) = v_i(t_0) + \int_{t_0}^{t_0+\Delta T} \left(\frac{V^{UHV}\left(\dot{s}_l(t)\right) - v_i(t)}{\tau} - \gamma\left(v_i(t) - v_{i+1}(t)\right) \right) dt \quad (11.)$$

Then, the discrete macroscopic traffic flow model for UHV could be formulated based on its car-following behavior. The desired speed in optimal velocity function $v_{f,i,j}^{UHV}$ is the expected speed of UHV drivers.

$$v_{i,j}^{UHV}(k+1) = v_{i,j}^{UHV}(k) + \frac{\Delta T}{\tau_i}\left[V_{i,j}^{UHV}\left(d_{i,j}^{ALL}(k)\right) - v_{i,j}^{UHV}(k)\right] + \frac{\Delta T}{L_i} v_{i,j}^{UHV}(k)\left[v_{i-1,j}^{UHV}(k) - v_{i,j}^{UHV}(k)\right] - \frac{v_i \Delta T}{\tau_i L_i} \frac{\left[d_{i+1,j}^{ALL}(k) - d_{i,j}^{ALL}(k)\right]}{\left[d_{i,j}^{ALL}(k)\right]} \quad (12.)$$

$$V_{i,j}^{UHV}\left[d_{i,j}^{ALL}(k)\right] = v_{f,i,j}^{UHV} \exp\left[-\frac{1}{a_{i,j}^{UHV}} \left(\frac{d_{i,j}^{ALL}(k)}{d_{cr,i,j}^{UHV}} \right)^{a_{i,j}^{UHV}} \right] \quad (13.)$$

Vehicle Type 4: LCHV

When the front vehicle decreases its speed, the car-following distance will decrease. Some vehicles will decrease their speed to keep a safe car-following status, while some drivers could make a lane-changing decision to keep a higher driving speed if the lane-changing conditions are satisfied on the adjacent lane. In the multi-lane mixed traffic environment, human drivers' lane-changing behavior could be triggered by the speed decreasing of front vehicle because of the VSL.

Lane-changing Analysis

1.Lane-changing Conditions

Generally, there are two lane-changing conditions for FVDM (*22*). It could be described as:

1. The distance between the new following vehicle on the target lane should be larger than the safe distance.

$$S_{safe} = s_0 + T\left[v_{\hat{f}} - \tau b_{safe} + \gamma\tau\left(v_{\hat{f}} - v_{LC}\right)\right] \quad (14.)$$

2. The distance between the new previous vehicle on the target lane should be larger than the advantage distance.

$$S_{adv} = s_f + T\tau[\Delta a + a_{bias} + \gamma(v_l - v_{\hat{l}})] \quad (15.)$$

where s_0 is the minimum acceptable following distance; s_f is the car-following distance on the current lane; $v_{\hat{f}}$, $v_{\hat{l}}$ is the traffic speed on the target lane; v_{LC} is the traffic speed of HV on the current lane; v_l is the speed of the CAV; Δa is the lane-changing threshold; a_{bias} is the asymmetry term; b_{safe} is the safe deceleration for drivers; T is the steady-state time gap; τ is the speed adaption time; and γ is sensitivity for speed differences.

Figure 1 illustrates the process for human drivers to make lane-changing decisions. When the lane-changing conditions are both satisfied, the HV could make a lane-changing decision to keep a higher driving speed.

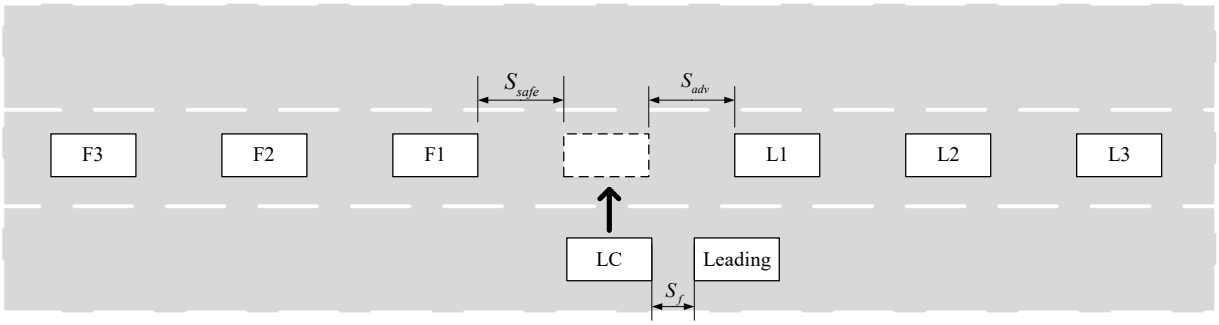

Figure 1 Lane-changing scenario for HV

2.Kinematic Analysis of LCHV

In a 10–15-minute time scale, the maneuver of lane-changing human-driven vehicles (LCHVs) could be divided into two parts: lane-changing and car-following after lane-changing. As a single lane-changing only takes 1-2 seconds, compared with the much larger predict time interval of 10-15 minutes, the short-time effect of lane-changing could be ignored, the car-following behavior of LCHV after lane-changing is mainly focused in this research.

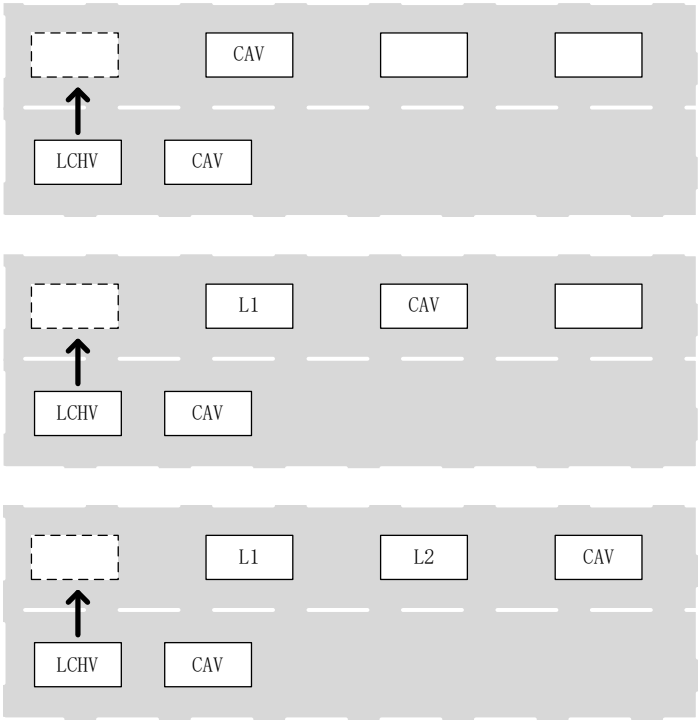

Figure 2 Vehicle Moving After Lane-Changing

After executing a lane change, the LCHV will align itself behind another vehicle in the adjacent lane. In the absence of a lane change, the HV should reduce its speed when the preceding vehicle in the current lane slows down. Due to the advantageous condition, the HV can maintain a higher speed in the adjacent lane after the lane change than in its original lane. Consequently, the subsequent movement of the LCHV is contingent upon the behavior of the new leading vehicle in the adjacent lane. As depicted in Figure 2, we observe that the further a CAV or a CHV is from the LCHV, the later the LCHV will decelerate its speed.

The vehicle (either CAV or CHV) influenced by the VSL will gradually decrease its speed as it approaches a VSL control spot. Consequently, the distance between the VSL-affected vehicle and the preceding vehicle will progressively increase until it reaches a value approximately equal to the current car-following distance. As a result, the VSL-affected vehicle can be considered the leader of a platoon, consisting of several UHVs that desire a higher speed but are also influenced by the deceleration of the VSL-affected vehicle, along with the LCHV itself. Moreover, in a given road segment, a higher proportion of VSL-affected vehicles leads to a shorter platoon length.

In this platoon, the moving of the leading vehicle could be described as:

$$\dot{v_{Lead}}(t) = \frac{V_{VSL}(t) - v_{Lead}(t)}{\tau} \tag{16.}$$

For the UHVs in the platoon following the VSL-affected vehicle, the car-following model could be written as:

$$\dot{v_i}(t) = \frac{V\left(\dot{s_i}(t)\right) - v_i(t)}{\tau} - \frac{v_i(t)}{L}\left(v_i(t) - v_{i+1}(t)\right) \tag{17.}$$

Considering the influence of the ratio of VSL-affected vehicles, the car-following model of LCHV could be derived. If there are 3 vehicles before the LCHV, the first vehicle is a VSL-affected vehicle, and the second and third vehicles are UHV. Then, the car-following model of the LCHV could be written as:

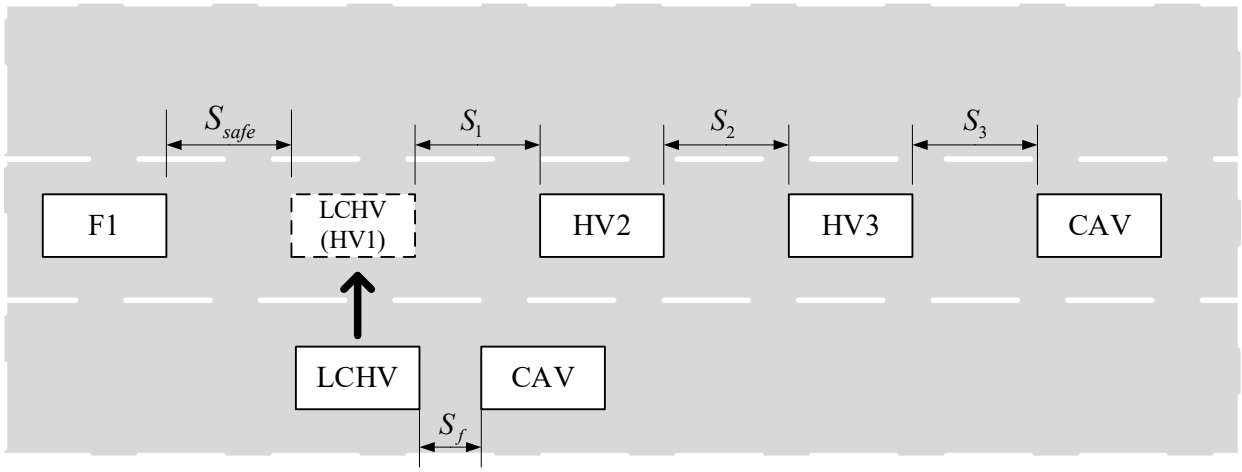

Figure 3 The situation of 3 vehicles before the LCHV

$$\dot{v_{LCHV}}(t, N=3) = \sum_{n=1}^{3}\left(\left(\frac{\Delta t}{L}\right)^{n-1}\left(\frac{V\left(\dot{s_n}(t)\right) - v_n(t)}{\tau} - \frac{v_n(t)(v_n(t) - v_{n+1}(t))}{L}\right)\prod_{n=1}^{2} v_n(t)\right) \tag{18.}$$

Then, after the iteration, if there are N vehicles before an LCHV. The leading vehicle is a VSL-affected vehicle, and the $N-1$ followed vehicles are UHV. The acceleration function of time could be written as:

$$\dot{v_{LCHV}}(t, N) = \sum_{n=1}^{N}\left(\left(\frac{\Delta t}{L}\right)^{n-1}\left(\frac{V\left(\dot{s_n}(t)\right) - v_n(t)}{\tau} - \frac{v_n(t)(v_n(t) - v_{n+1}(t))}{L}\right)\prod_{n=1}^{N-1} v_n(t)\right) \tag{19.}$$

That (Equ 19) is the microscopic car-following model for the LCHV following a N vehicle platoon after the lane-changing. The penetration rate of CAVs is α on a freeway segment, then, the probability for

following an N-vehicle platoon is $\alpha(1-\alpha)^{N-1}$. Generally, by adding all possible situations together, the acceleration function for the LCHV is:

$$\dot{v_{LCHV}}(t) = \sum_{N=1}^{\infty} \alpha(1-\alpha)^{N-1} \sum_{n=1}^{N} \left(\left(\frac{\Delta t}{L}\right)^{n-1} \left(\frac{V\left(\dot{s_n}(t)\right) - v_n(t)}{\tau} - \frac{v_n(t)\left(v_n(t) - v_{n+1}(t)\right)}{L} \right) \prod_{n=1}^{N-1} v_n(t) \right) \quad (20.)$$

where N is the number of vehicles in the platoon before a LCHV, including one VSL-compliant vehicle and $N-1$ VSL-uncompliant vehicles; α is the penetration rate of CAV; L is the length of the road segment; τ is the speed adaption time; Δt is a little o number $\dot{s_n}(t)$ is the car-following distance for vehicle n at time t; $v_n(t)$ is the speed of vehicle n at time t, and:

$$v_n(t) = \begin{cases} v_{LCHV}(t) & n = 1 \\ v_n(t) & otherwise \\ v_{Lead}(t) & n = N+1 \end{cases}$$

Similarly, for road segment i and lane j at time interval $k+1$ the discrete macroscopic traffic flow model of LCHV could be written as:

$$v_{i,j}^{LCHV}(k+1) = v_{i,j}^{LCHV}(k) - \frac{v_i \Delta T}{\tau_i L_i} \frac{\left[d_{i+1,j}^{ALL}(k) - d_{i,j}^{ALL}(k)\right]}{\left[d_{i,j}^{ALL}(k)\right]} + \Delta T \sum_{N=1}^{\infty} \alpha_{i,j}(1-\alpha_{i,j})^{N-1} \times$$

$$\sum_{n=1}^{N} \left(\left(\frac{\Delta t}{L_i}\right)^{n-1} \left(\frac{V_{i,j}^{LCHV}\left(d_{i,j}^{ALL}(k)\right) - v_{i,j}^{LCHV}(k)}{\tau_i} + \frac{v_{i,j}^{LCHV}(k)\left(v_{i-1,j}^{HV}(k) - v_{i,j}^{LCHV}(k)\right)}{L_i} \right) \prod_{n=1}^{N-1} v_{i,j}^{LCHV}(k) \right) \quad (21.)$$

The optimal velocity function of LCHV is related to $v_{f,i,j}^{LCHV}$, which is the driver's expected speed of LCHV.

$$V_{i,j}^{LCHV}\left[d_{i,j}^{ALL}(k)\right] = v_{f,i,j}^{LCHV} \exp\left[-\frac{1}{a_{i,j}^{LCHV}} \left(\frac{d_{i,j}^{ALL}(k)}{d_{cr,i,j}^{LCHV}} \right)^{a_{i,j}^{LCHV}} \right] \quad (22.)$$

3. Proportion Analysis

The proportion of LCHV is related to the traffic flow status and lane-changing conditions. Human drivers are assumed to be greedy. As long as the lane-changing conditions are satisfied, the driver will change lanes to ensure that the driving speed will not be affected by the deceleration of the leading vehicle. Drivers are also assumed to change their lanes only once per time interval.

For two homogeneous adjacent lanes m and $m+1$, if the vehicle on lane m intend to switch to lane $m+1$, the vehicle space on lane $m+1$ $s_{m+1}^{Initial}$ should be larger than:

$$S_{m,m+1}^{Initial} = s_0 + T\left[v_{m+1}^{Initial} + \tau\left(\Delta a + a_{bias} - b_{safe}\right)\right] + s_m^{Initial} \quad (23.)$$

Then, $n_{m,m+1}$ human-drivers will change their lane from m to $m+1$, the final HV number on lane $m+1$ after lane-changing will be $n_{m+1}^{Initial} + n_{m,m+1}$, and the HV number of lane m will be $n_m^{Initial} - n_{m,m+1}$ The traffic density after lane-changing for lane m and $m+1$ could be $\frac{n_m^{Initial} - n_{m,m+1}}{L}$ and $\frac{n_{m+1}^{Initial} + n_{m,m+1}}{L}$ respectively; and car-following distance after lane-changing for lane m and $m+1$ is $\frac{L}{n_m^{Initial} - n_{m,m+1}}$ and $\frac{L}{n_{m+1}^{Initial} + n_{m,m+1}}$.

Because the drivers are greedy, the final traffic state of lane $m+1$, which is the vehicle distance on lane $m+1$ s_{m+1}^{Final} should be equal to:

$$S_{m,m+1}^{Final} = s_0 + T\left[v_{m+1}^{Final} + \tau\left(\Delta a + a_{bias} - b_{safe}\right)\right] + s_m^{Final} \quad (24.)$$

The number of lane-changing vehicles from lane m to lane $m+1$ is $n_{m,m+1}$, the number of lane-changing is related to the traffic flow status on the target lane. Then, we have

$$0 = s_0 + T\left[v_{f,i,m+1}\exp\left[-\frac{1}{a_{i,m+1}}\left(\frac{n_{m+1}^{Initial} + n_{m,m+1}}{Ld_{cr,i,m+1}}\right)^{a_{i,m+1}}\right] + \tau\left(\Delta a + a_{bias} - b_{safe}\right)\right] + \frac{L}{n_m^{Initial} - n_{m,m+1}} - \frac{L}{n_{m+1}^{Initial} + n_{m,m+1}} \quad (25.)$$

Then, in road segment i, the proportion of LCHVs from lane m to lane $m+1$ is

$$\omega_{i,m,m+1} = \frac{n_{m,m+1}}{n_m^{Initial}} \quad (26.)$$

where, $\omega_{i,m,m+1}$ is the proportion of LCHVs from lane m to lane $m+1$ in road segment i; $n_{m+1}^{Initial}$ is the initial vehicle number in the road segment on lane $m+1$; $n_m^{Initial}$ is the initial vehicle number in the road segment on lane m; $n_{m,m+1}$is the number of vehicles change their lane from lane m to lane $m+1$; L is the length of the road segment; s_0 is the minimum acceptable following distance; T is the steady-state time gap; τ is the speed adaption time; Δa is the lane-changing threshold; a_{bias} is the asymmetry term; b_{safe} is the safe deceleration for drivers; $v_{f,i,m+1}$is the expected velocity for vehicles on segment i lane $m+1$; $d_{cr,i,m+1}$ is the critical density on road segment i and lane $m+1$; and $a_{i,m+1}$ is the speed exponent term of segment i and lane $m+1$ for HVs.

Then, for a macroscopic level, at time interval k the density changes from lane j to lane $j+1$ because of LCHV $d_{i,j,j+1}(k)$ on segment i could be formulated as:

$$f(d_{i,j,j+1}(k)) = s_0 + \Delta T\left[v_{f,i,j+1}^{Veh}\exp\left[-\frac{1}{a_{i,j+1}^{Veh}}\left(\frac{d_{i,j+1}^{ALL}(k) + d_{i,j,j+1}(k)}{L_i^2 d_{cr,i,j+1}^{Veh}}\right)^{a_{i,j+1}^{Veh}}\right] + \tau\left(\Delta a + a_{bias} - b_{safe}\right)\right] + \frac{1}{d_{i,j}^{ALL}(k) - d_{i,j,j+1}(k)} - \frac{1}{d_{i,j+1}^{ALL}(k) + d_{i,j,j+1}(k)} \quad (27.)$$

At time interval k, the proportion of LCHVs from lane j to lane $j+1$ on segment i is:

$$\omega_{i,j,j+1}(k) = \frac{d_{i,j,j+1}(k)}{d_{i,j}^{ALL}(k)} \quad (28.)$$

The Summary of Discrete Macroscopic Multi-class Traffic Model

Based on the kinematic analysis of CAVs, CHVs, UHVs, and LCHVs in this section, the second-order multi-class discrete macroscopic traffic flow model proposed in this research could be summarized as follows:

$$v_{i,j}(k+1) = \alpha_{i,j}(k)v_{i,j}^{CAV}(k+1) + \beta_{i,j}(k)v_{i,j}^{UHV}(k+1) + \left(1 - \alpha_{i,j}(k) - \beta_{i,j}(k) - \omega_{i,j,j+1}(k) - \omega_{i,j,j-1}(k)\right)v_{i,j}^{CHV}(k+1) + \left(\omega_{i,j+1,j}(k) + \omega_{i,j-1,j}(k)\right)v_{i,j}^{LCHV}(k+1) \quad (29.)$$

$$v_{i,j}^{CAV}(k+1) = v_{i,j}^{CAV}(k) + \frac{\Delta T}{\tau_i}\left[V_{i,j}^{CAV}\left(d_{i,j}^{ALL}(k)\right) - v_{i,j}^{CAV}(k)\right] + \frac{\Delta T}{L_i} v_{i,j}^{CAV}(k)\left[v_{i-1,j}^{CAV}(k) - v_{i,j}^{CAV}(k)\right] - \frac{\nu_i \Delta T}{\tau_i L_i}\frac{\left[d_{i+1,j}^{ALL}(k) - d_{i,j}^{ALL}(k)\right]}{\left[d_{i,j}^{ALL}(k) + \kappa_i\right]} \quad (30.)$$

$$v_{i,j}^{HV}(k+1) = v_{i,j}^{HV}(k) + \frac{\Delta T}{\tau_i}\left[V_{i,j}^{HV}\left(d_{i,j}^{ALL}(k)\right) - v_{i,j}^{HV}(k)\right] + \frac{\Delta T}{L_i} v_{i,j}^{HV}(k)\left[v_{i-1,j}^{HV}(k) - v_{i,j}^{HV}(k)\right] - \frac{\nu_i \Delta T}{\tau_i L_i}\frac{\left[d_{i+1,j}^{ALL}(k) - d_{i,j}^{ALL}(k)\right]}{\left[d_{i,j}^{ALL}(k) + \kappa_i\right]} \quad (31.)$$

$$v_{i,j}^{LCHV}(k+1) = v_{i,j}^{LCHV}(k) - \frac{\nu_i \Delta T}{\tau_i L_i}\frac{\left[d_{i+1,j}^{ALL}(k) - d_{i,j}^{ALL}(k)\right]}{\left[d_{i,j}^{ALL}(k)\right]} + \Delta T \sum_{N=1}^{\infty} \alpha_{i,j}(1-\alpha_{i,j})^{N-1} \times \sum_{n=1}^{N}\left(\left(\frac{\Delta t}{L_i}\right)^{n-1}\left(\frac{V_{i,j}^{LCHV}\left(d_{i,j}^{ALL}(k)\right) - v_{i,j}^{LCHV}(k)}{\tau_i} + \frac{v_{i,j}^{LCHV}(k)\left(v_{i-1,j}^{HV}(k) - v_{i,j}^{LCHV}(k)\right)}{L_i}\right)\prod_{n=1}^{N-1} v_{i,j}^{LCHV}(k)\right) \quad (32.)$$

$$V_{i,j}^{Veh}\left[d_{i,j}^{ALL}(k)\right] = v_{f,i,j}^{Veh}\exp\left[-\frac{1}{a_{i,j}^{Veh}}\left(\frac{d_{i,j}^{ALL}(k)}{d_{cr,i,j}^{Veh}}\right)^{a_{i,j}^{Veh}}\right] \quad (33.)$$

$$\omega_{i,j,j+1}(k) = \frac{d_{i,j,j+1}(k)}{d_{i,j}^{ALL}(k)} \quad (34.)$$

$$f\left(d_{i,j,j+1}(k)\right) = s_0 + \Delta T\left[v_{f,i,j+1}^{Veh}\exp\left[-\frac{1}{a_{i,j+1}^{Veh}}\left(\frac{d_{i,j+1}^{ALL}(k) + d_{i,j,j+1}(k)}{L_i^2 d_{cr,i,j+1}^{Veh}}\right)^{a_{i,j+1}^{Veh}}\right] + \tau\left(\Delta a + a_{bias} - b_{safe}\right)\right] + \frac{1}{d_{i,j}^{ALL}(k) - d_{i,j,j+1}(k)} - \frac{1}{d_{i,j+1}^{ALL}(k) + d_{i,j,j+1}(k)} \quad (35.)$$

$$d_{i,j}^{ALL}(k) = d_{i,j}^{CAV}(k) + d_{i,j}^{HV}(k) \quad (36.)$$

$$d_{i,j}^{CAV}(k+1) = d_{i,j}^{CAV}(k) + \frac{\Delta T}{L_i}\left[q_{i-1,j}^{CAV}(k) - q_{i,j}^{CAV}(k) + r_{i,j}^{CAV}(k) - s_{i,j}^{CAV}(k)\right] \quad (37.)$$

$$d_{i,j}^{HV}(k+1) = d_{i,j}^{HV}(k) + \frac{\Delta T}{L_i}\left[q_{i-1,j}^{HV}(k) - q_{i,j}^{HV}(k) + r_{i,j}^{HV}(k) - s_{i,j}^{HV}(k)\right] - d_{i,j,j+1}(k) - d_{i,j,j-1}(k) + d_{i,j+1,j}(k) + d_{i,j-1,j}(k) \quad (38.)$$

$$q_{i,j}^{ALL}(k) = q_{i,j}^{CAV}(k) + q_{i,j}^{HV}(k) \quad (39.)$$

$$q_{i,j}^{CAV}(k) = d_{i,j}^{CAV}(k) v_{i,j}^{CAV}(k) \quad (40.)$$

$$q_{i,j}^{HV}(k) = d_{i,j}^{HV}(k) v_{i,j}^{HV}(k) \quad (41.)$$

NEUMERICAL EXPERIMENT

In order to assess the performance of the multi-class METANET (MultiMETANT) model proposed in this research, a series of numerical experiments are conducted. The primary focus of these experiments revolves around the estimation of traffic on a 3-lane highway, wherein varying VSL settings are employed within a mixed traffic environment. This section comprehensively elucidates the design of the numerical experiments concerning freeway geometry, mixed traffic flow simulation, model parameters, and measurements.

Freeway Geometry

In the experiment, we have designed a 3-lane straight freeway with mixed traffic flow for model evaluation. The total length of this study area measures 5 km, divided into 5 segments, each spanning 1 km. Within this mixed traffic environment, we have a combination of CAVs and HVs. The HVs are capable of both car-following and lane-changing maneuvers.

As Figure 4 shows, the sensors are installed along the roadside for data collection. Additionally, a speed control board is strategically positioned at the beginning of segment 3, indicating that segment 3 is the initial road segment where speed control measures are implemented.

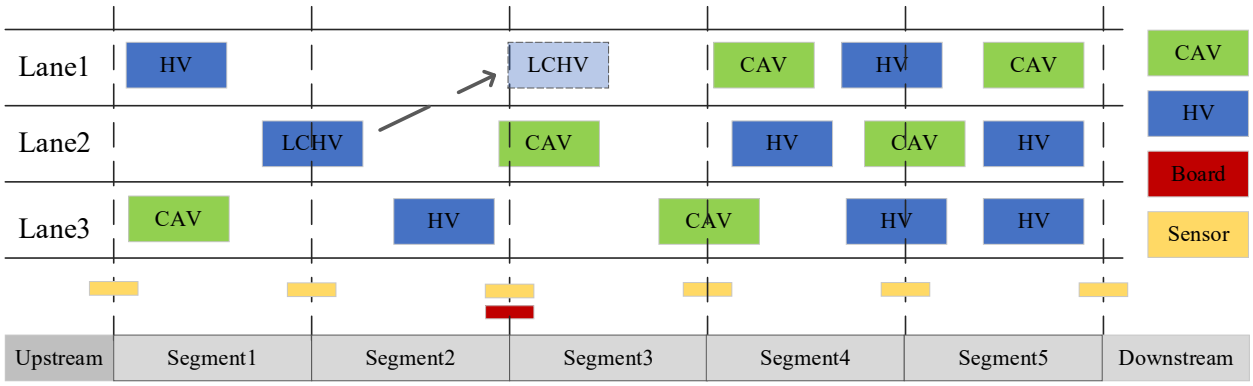

Figure 4 Geometry of experiment road

Mixed Traffic Flow Generator

The traffic flow analyzed in this research is generated by a simulator. Within the traffic flow, vehicles are observed to move using the FVDM. Additionally, vehicles have the capability to change lanes provided that the lane-changing conditions are met. The CAV and CHV vehicles will adjust their desired speed to speed control requirements, whereas the LCHV and UHVs will maintain their desired speed as the free flow speed regardless of whether they are in a speed control segment.

The traffic trajectory data was generated using a mixed traffic flow simulator comprising Connected and Autonomous Vehicles (CAVs) and Human-driven Vehicles (HVs). The total simulation duration lasted 3900 seconds, and the effective area covered a distance of 5000 meters. A specific speed control location was designated at 2000 meters.

Parameters

Table 1 Value of parameters

Parameter	Value
Vehicle Simulator	
s_0	3m
b_{safe}	$2m/s^2$
b_{max}	$5m/s^2$
b_{sharp}	$8m/s^2$
τ	5s
T	2s
γ	0.6
Δa	$5m/s^2$
a_{max}	$5m/s^2$
u_f	120 km/h
METANET and MultiMETANET	
τ	*20* s
ν	0.05
κ	13 veh/km/lane
u_f	120 km/h
d_{cr}	33.5 veh/km
a	1.4324
α	0.2

The parameters employed in the experiment for both the vehicle trajectory simulator and the traffic model are documented in

Table 1. The parameters utilized in the vehicle simulator serve to produce vehicle trajectories in a mixed traffic environment. The parameters for METANET(*23*) and MultiMETANET are configured to evaluate the performance of the traffic model.

Measurements

To evaluate the performance of the proposed multi-class METANET model, the error metrics Root Mean Squared Error (RMSE), Mean Absolute Percentage Error (MAPE), Mean Squared Prediction Error (MSPE), and Root Mean Squared Prediction Error (RMSPE) are applied. The definitions of the error metrics are shown in the following equations.

$$RMSE = \sqrt{\frac{1}{N}\sum_{i=1}^{N}(x_i - \hat{x}_i)^2} \tag{42.}$$

$$MAPE = \frac{1}{N}\sum_{i=1}^{N}\left|\frac{x_i - \hat{x}_i}{\hat{x}_i}\right| \tag{43.}$$

$$MSPE = \frac{1}{N}\sum_{i=1}^{N}\left(\frac{x_i - \hat{x}_i}{\hat{x}_i}\right)^2 \tag{44.}$$

$$RMSPE = \sqrt{\frac{1}{N}\sum_{i=1}^{N}\left(\frac{x_i - \widehat{x_i}}{\widehat{x_i}}\right)^2} \quad (45.)$$

where $\widehat{x_i}$ represents the value of estimation of mixed traffic flow model at each time step i; and x_i denotes the traffic flow data generated by the simulator.

RESULTS DISCUSSION

Effectiveness Analysis

Figure 5 illustrates the time-space pattern of vehicles in each lane, depicting their trajectories and corresponding speeds. Initially, all vehicles were configured with an initial speed of 120 km/h, and the speed was controlled to decrease to 80 km/h after passing the designated control spot at 2000 meters. Clearly, the figure shows a distinct decrease in the slope of vehicle trajectories, indicating a reduction in vehicle speed following the control point. Furthermore, the figure reveals that lane 2 exhibited a higher initial traffic density compared to lanes 1 and 3. As a result, vehicles in lanes with higher initial density, such as lane 2, demonstrated a greater tendency to switch to lanes with lower density after receiving the speed decrease command.

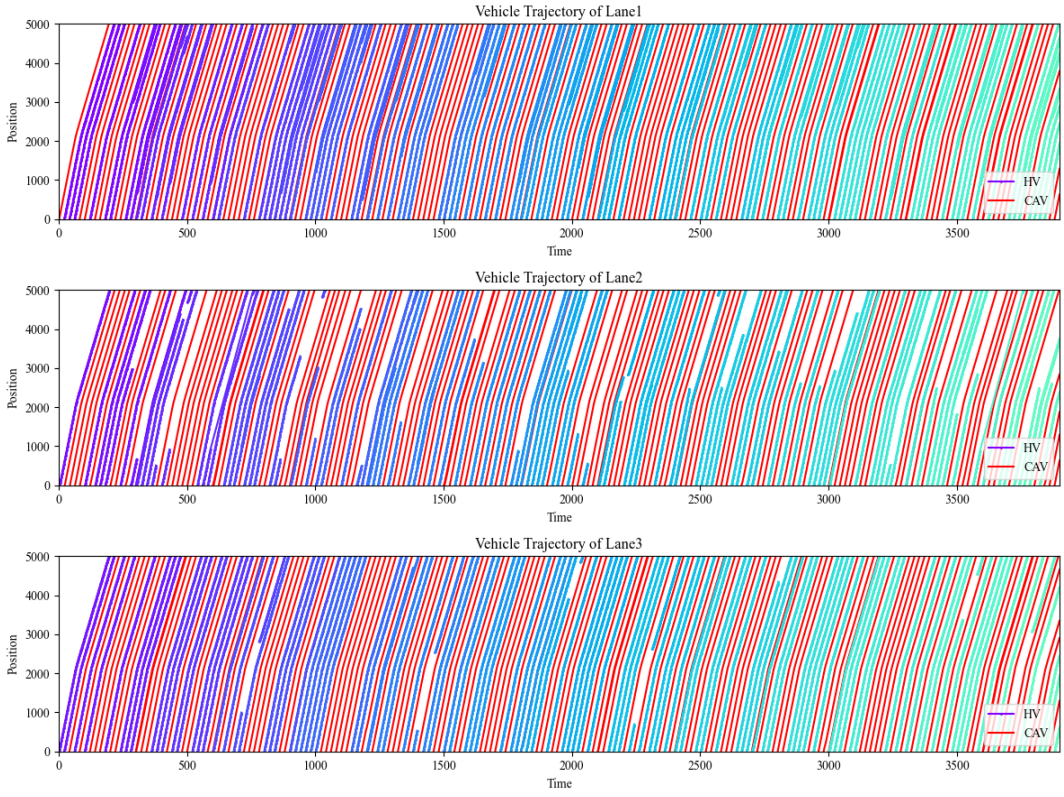

Figure 5 Vehicle trajectory in 3 lanes simulation

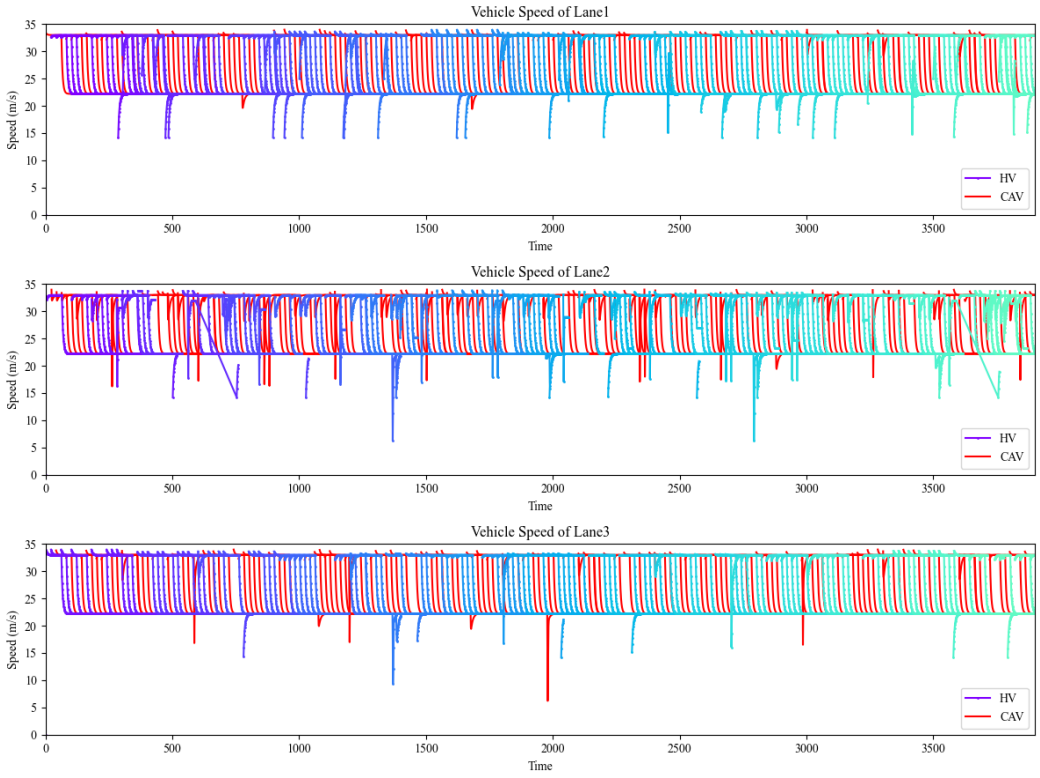

Figure 6 Vehicle speed in 3 lanes simulation

The traffic status data is obtained from the vehicle trajectory data generated by the mixed traffic flow simulator. To evaluate the effectiveness of the multi-class traffic model presented in this study, we utilize the original METANET model as the reference for traffic status prediction.

Figure 7 illustrates the model's performance in traffic flow estimation. It is evident that the predictive outcomes of the multi-class model closely match the actual traffic flow, outperforming the original METANET model. Notably, substantial improvements in the multi-class model's performance are observed, particularly after vehicle speed control, in segments 2, 3, and 4.

The proposed model shows a considerable improvement in traffic speed estimation. This enhancement is visually evident from Figure 8, where it becomes apparent that the Multiclass METANET outperforms the original METANET in accurately depicting the variable speed limit (VSL). Notably, after passing the control spot, the majority of vehicles adhere to the speed limitation. In contrast to the original METANET's speed estimation, which indicates an increase over time in speed along road sections after speed control, the proposed multi-class traffic model demonstrates a decrease in speed due to the influence of VSL.

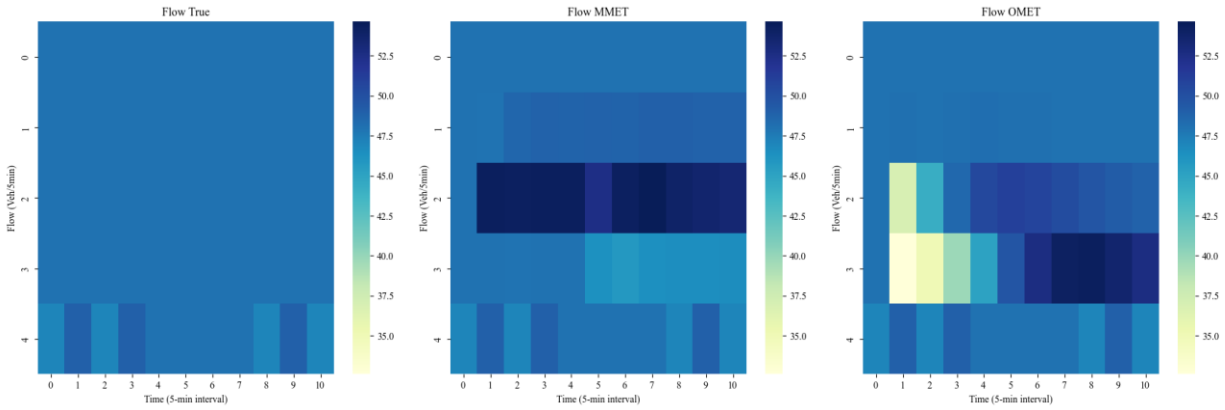

Figure 7 Traffic flow estimation

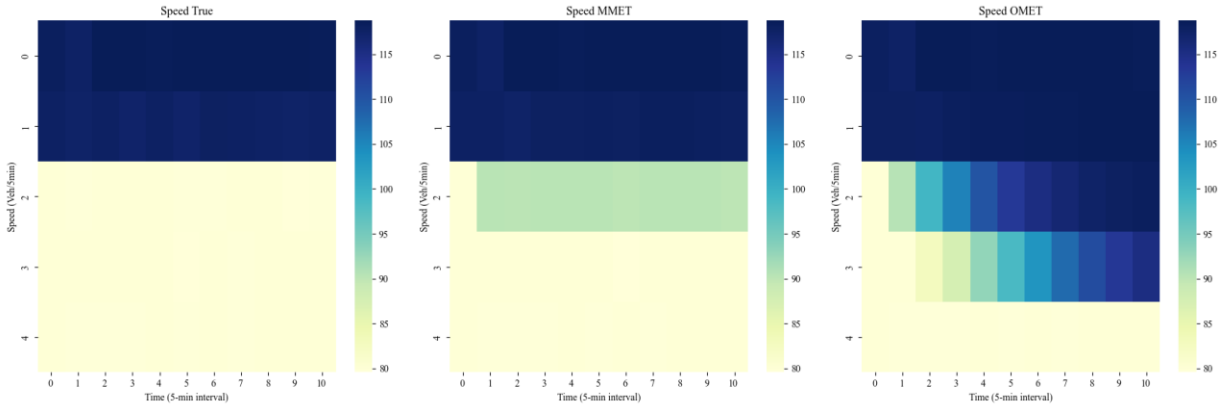

Figure 8 Speed estimation

Table 2 Errors of model prediction

	Traffic Flow		Traffic Speed	
	MultiMETANET	METANET	MultiMETANET	METANET
RMSE	2.626936	3.830534	4.466233	16.7441
MAPE	0.02925	0.037628	0.024635	0.115122
MSPE	0.002997	0.006373	0.002122	0.029819
RMSPE	0.054728	0.079803	0.055906	0.209676

In this case, the MultiMETANET model achieved a substantially lower root mean square error (RMSE) of 2.626936 in traffic flow estimation, while the METANET model obtained a higher RMSE of 3.830534. Similarly, in traffic speed estimation, MultiMETANET obtained an RMSE of 4.466233, whereas the METANET model had a significantly higher RMSE of 16.7441. The lower RMSE values indicate that the MultiMETANET model outperforms the METANET model in accurately predicting traffic-related values.

MAPE computes the average percentage difference between predicted values and actual values. The results show that the MultiMETANET model outperforms the METANET model in both traffic flow and traffic speed prediction. The MAPE for MultiMETANET is 0.02925 in traffic flow estimation and 0.024635 in the traffic speed prediction. In contrast, the METANET model yields higher MAPE values of 0.037628 and 0.115122 in the traffic flow and speed prediction, respectively. The lower MAPE values for MultiMETANET indicate that it provides more accurate predictions with smaller percentage errors. MSPE measures the average squared percentage differences between predicted and actual values. Once again, the MultiMETANET model demonstrates superior performance, as it achieves lower MSPE values in both scenarios. The MultiMETANET's MSPE values are 0.002997 and 0.002122 in flow and speed estimation, respectively. On the other hand, the METANET model has higher MSPE values of 0.006373 and 0.029819 in the flow and speed estimation, respectively. The lower MSPE values for MultiMETANET highlight its ability to provide more precise predictions with minimized squared percentage errors. RMSPE computes the square root of the average squared percentage differences between predicted and actual values. As with the other metrics, the MultiMETANET model performs better in this evaluation as well. It achieves RMSPE values of 0.054728 and 0.055906, while the METANET model has higher RMSPE values of 0.079803 and 0.209676 in flow and speed prediction respectively. The lower RMSPE values for MultiMETANET indicate its superior accuracy in predicting traffic-related values with minimized percentage errors.

In conclusion, the proposed model, by capturing the lane-changing behavior of HVs, offers a more comprehensive representation of the traffic status compared to the original METANET model, encompassing both speed and flow. The analysis of the performance metrics demonstrates that the MultiMETANET model outperforms the METANET model in both traffic flow estimation and traffic speed prediction. It consistently exhibits lower values across all evaluation metrics, highlighting its superiority in accurately estimating traffic status.

Sensitive Analysis of VSL Difference

To further investigate the model's performance under various differences in VSL (Variable Speed Limit) speeds, the experiments encompass diverse traffic flow scenarios. Specifically, the initial traffic speed is set at 120 km/h, while the speed limit assumes different lower values (110 km/h, 100 km/h, 90 km/h, 80 km/h, and 70 km/h). The analysis primarily centers on evaluating the extent of performance enhancement using RMSE, MAPE, MSPE, and RMSPE.

With different VSL speeds, Figure 9 illustrates the model's performance in estimating traffic flow, while Figure 10 displays the predictions of traffic speed. Concerning traffic flow estimation, it is evident that as the disparity between the Variable Speed Limit (VSL) and free flow speed increases, the flow variance at speed control section 2 becomes more pronounced. This is attributed to the greater influence of the speed limit on the traffic flow with a larger difference in VSL. Regarding traffic speed estimation, as the speed difference expands, the variance of the predicted speed also increases, indicating the model's effectiveness in predicting speed across different VSL values.

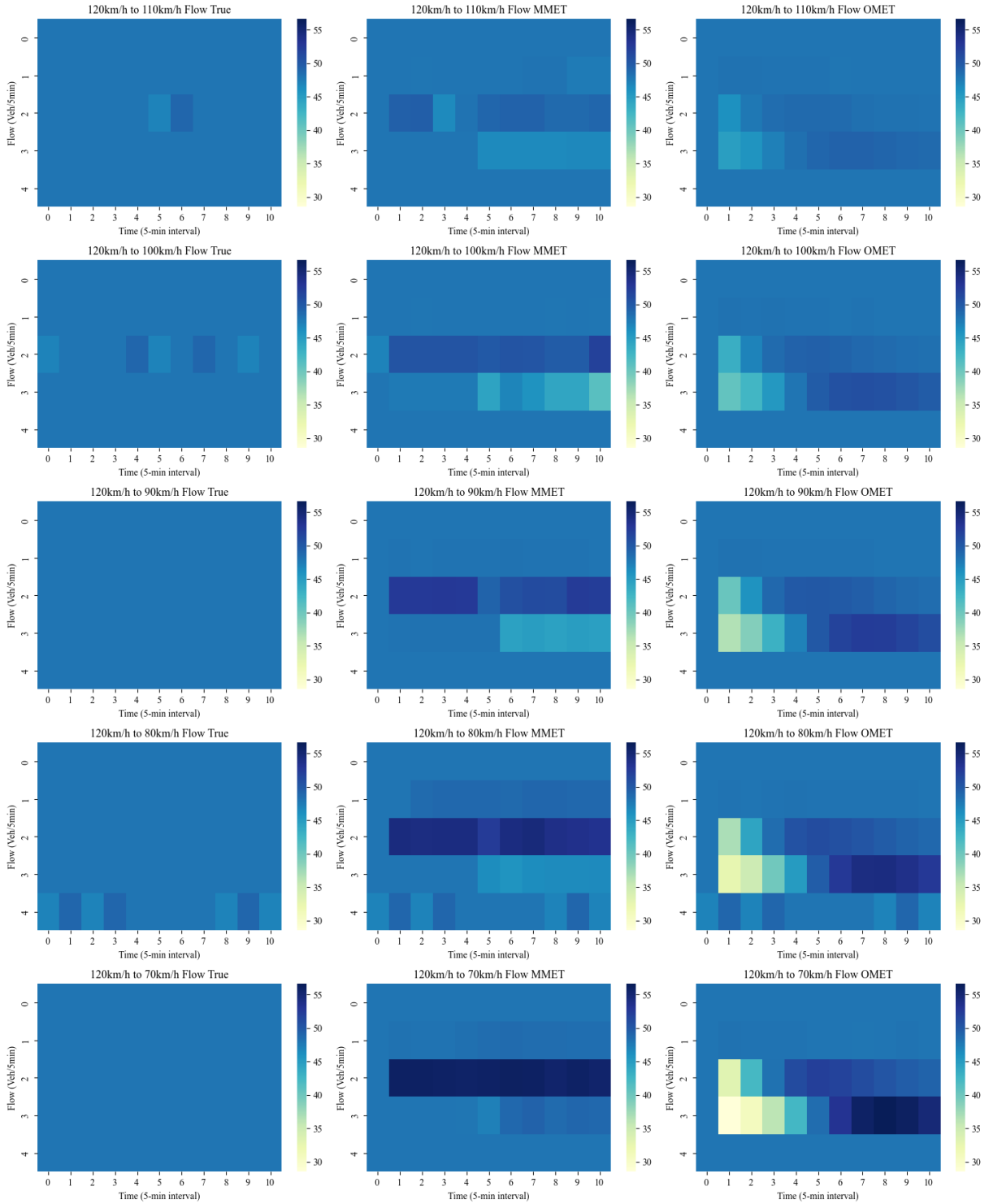

Figure 9 Traffic flow estimation with different VSL speed

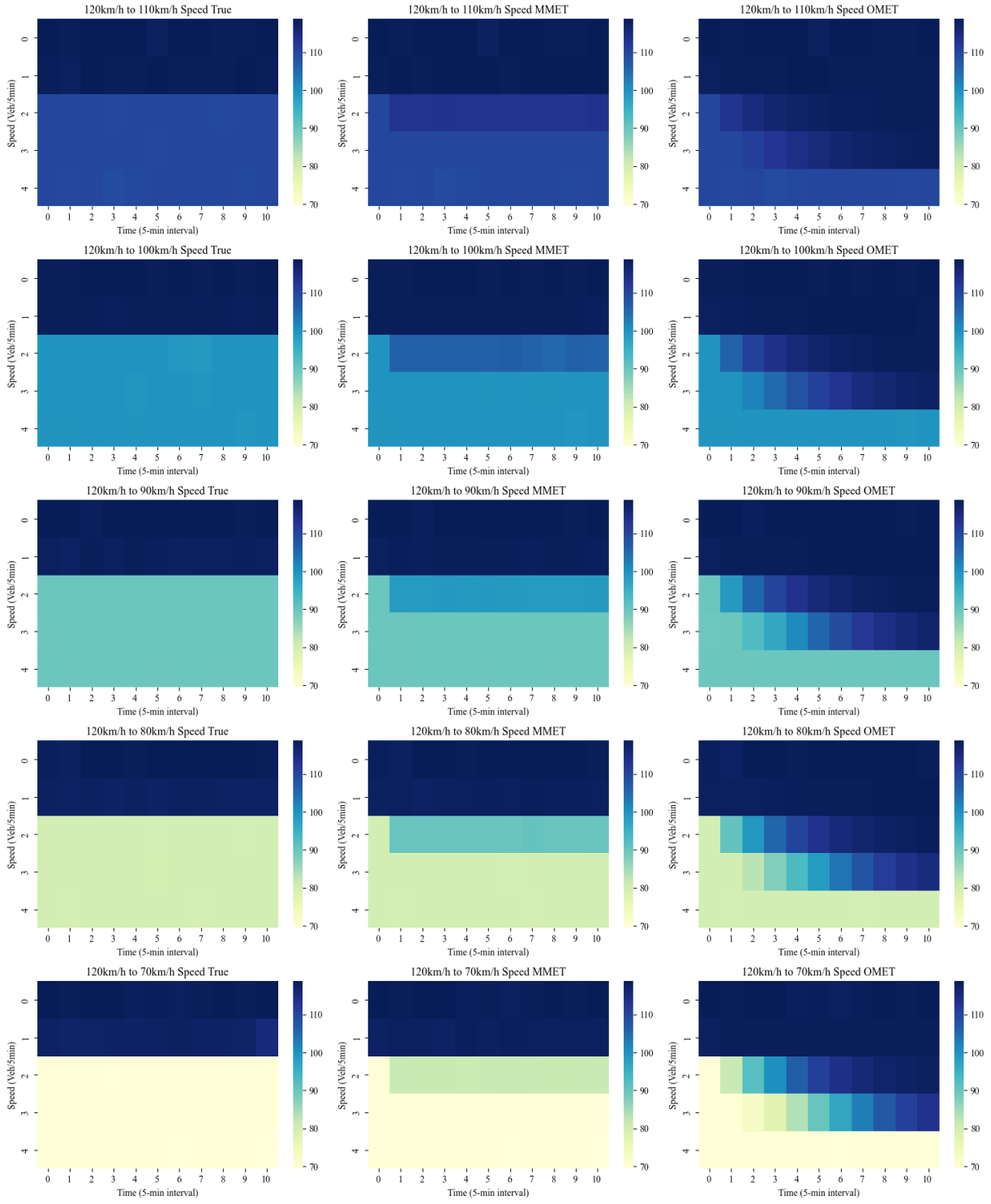

Figure 10 Traffic speed estimation with different VSL speed

Table 3 Errors of model prediction with different VSL speed

	Traffic Flow			Traffic Speed		
	Multi METANET	**METANET**	**Improvement**	**Multi METANET**	**METANET**	**Improvement**
120km/h to 110 km/h						
RMSE	0.701197	0.755647	7.21%	1.435452	4.069715	64.73%
MAPE	0.007824	0.007795	-0.37%	0.00587	0.020998	72.04%
MSPE	0.000213	0.000248	13.89%	0.00016	0.001289	87.56%
RMSPE	0.014653	0.015773	7.10%	0.013076	0.03708	64.74%
120km/h to 100 km/h						
RMSE	1.694786	1.697376	0.15%	2.771797	8.681826	68.07%
MAPE	0.017818	0.016763	-6.29%	0.01234	0.048785	74.71%
MSPE	0.001248	0.001251	0.30%	0.000664	0.006516	89.81%
RMSPE	0.035372	0.035404	0.09%	0.027841	0.087197	68.07%
120km/h to 90 km/h						
RMSE	1.942346	2.691084	27.82%	3.734368	12.77466	70.77%
MAPE	0.021094	0.026262	19.68%	0.01832	0.07883	76.76%
MSPE	0.001637	0.003143	47.90%	0.001334	0.01561	91.45%
RMSPE	0.040466	0.056064	27.82%	0.041478	0.141936	70.78%
120km/h to 80 km/h						
RMSE	2.626936	3.830534	31.42%	4.466233	16.7441	73.33%
MAPE	0.02925	0.037628	22.26%	0.024635	0.115122	78.60%
MSPE	0.002997	0.006373	52.97%	0.002122	0.029819	92.89%
RMSPE	0.054728	0.079803	31.42%	0.055906	0.209676	73.34%
120km/h to 70 km/h						
RMSE	3.342379	5.111124	34.61%	4.947461	20.38392	75.73%
MAPE	0.033142	0.050117	33.87%	0.031353	0.158486	80.22%
MSPE	0.004849	0.011338	57.24%	0.002888	0.049022	94.11%
RMSPE	0.069633	0.106482	34.61%	0.070755	0.291951	75.76%

Table 3 reveals that the model's performance for both traffic flow and traffic speed estimation deteriorates (increased RMSE, MAPE, MSPE, and RMSPE) with a reduction in the speed limit from 120 km/h to 70 km/h. In contrast, the improvement demonstrated by MultiMETANET over the benchmark shows a progressive trend. This can be attributed to the fact that as the speed difference of Variable Speed Limits (VSL) increases, there is a subsequent rise in the number of lane-changing events caused by the speed decrease of the leading vehicles. Consequently, the MultiMETANET model proposed in this research, which takes into account the behavior of lane-changing vehicles, allows for a more accurate representation of the traffic flow status.

Regarding the traffic flow estimation, the MultiMETANET exhibits superior performance compared to the original METANET. The extent of improvement increases as the speed difference grows larger, leading to improvements of 34.61% in RMSE, 33.87% in MAPE, 57.24% in MSPE, and 34.61% in RMSE, respectively.

Concerning the speed estimation, the MultiMETANET also demonstrates significant enhancements over the benchmark. Notably, it exhibits greater improvements compared to the traffic flow estimation. This outcome can be attributed to the model proposed based on kinematic analysis of various vehicle categories, enabling the MultiMETANET model proposed in this research to more accurately describe vehicle speeds and achieve superior overall performance.

CONCLUSIONS

The CAV technology holds promising benefits for road traffic management. In the long run, HVs and CAVs are expected to coexist and share the road network. To effectively support traffic management in this mixed traffic environment, it is essential to establish a fundamental traffic model theory. However, the conventional macroscopic traffic model faces critical challenges that need to be addressed, including (a) Incorporating the lane-changing and car-following behaviors of HVs into the macroscopic traffic flow model to accurately capture the interaction between CAVs and HVs. (b) Developing a model for variable speed limit control that effectively accommodates both CAVs and HVs in a mixed traffic environment. (c) Properly accounting for the impact of the penetration rate and compliant rate of CAVs on the dynamics of traffic flow in freeway scenarios. Addressing these critical issues is essential to devise comprehensive traffic management strategies and ensuring the seamless integration of CAVs and HVs in mixed traffic environments.

In this study, we introduce a discrete second-order macroscopic traffic model to bridge the existing gap. The proposed model categorizes vehicles into distinct classes, each possessing unique characteristics. Formulating the macroscopic model relies on the microscopic movement of each vehicle class, taking into account essential factors such as lane-changing and car-following behaviors. Additionally, the model effectively captures the intricate interaction between Connected and Autonomous Vehicles (CAVs) and Human-Operated Vehicles (HVs) arising from speed control. Moreover, both the penetration rate of CAVs and the compliant rate of HVs are incorporated into the framework of this model, contributing to its comprehensive and realistic representation of mixed traffic dynamics.

The numerical experiment was conducted to validate the performance of the proposed MultiMETANET model. When compared to the original METANET model, the proposed model demonstrates a higher degree of accuracy in predicting traffic status. Specifically, in terms of traffic flow estimation, the MultiMETANET exhibits significantly superior performance to the original METANET, with remarkable enhancements observed across the evaluation metrics. These improvements include a 34.61% reduction in RMSE, a 33.87% decrease in MAPE, a 57.24% decrease in MSPE, and a 34.61% decrease in RMSE, respectively. Regarding speed estimation, the MultiMETANET also showcases substantial advancements over the benchmark, surpassing the improvements observed in traffic flow estimation. This outcome can be attributed to the MultiMETANET model being designed based on kinematic analysis of various vehicle categories, enabling it to more accurately capture vehicle speeds and achieve an overall superior performance compared to the original METANET model.

The proposed model holds the potential to facilitate various traffic control tasks in freeway management. By effectively estimating the mixed traffic status through current speed control on both CAVs and HVs, the model can contribute to more efficient traffic management strategies. Since the proposed model has been exclusively tested with a base case of a 20% CAV penetration rate, exploring the effects of different penetration rates of CAVs could be a valuable subject for future research. Investigating pertinent issues related to varying rates of CAVs would offer valuable insights and enhance our understanding of the model's performance under different scenarios, thereby contributing to further advancements in traffic flow management in mixed traffic environments.

ACKNOWLEDGMENTS

This study is supported by the grant titled "CAREER: Physics Regularized Machine Learning Theory: Modeling Stochastic Traffic Flow Patterns for Smart Mobility Systems," funded by the National Science Foundation. The authors would like to acknowledge the utilization of ChatGPT, a large language model, exclusively for enhancing the linguistic quality of the manuscript preparation process.

AUTHOR CONTRIBUTIONS

The authors confirm contribution to the paper as follows: study conception and design: Y. Zhang, X. Yang; simulation and data collection: Y. Zhang, K. Yang, Y. Lei; analysis and interpretation of results: Y. Zhang, Y. Gong; draft manuscript preparation: Y. Zhang, X. Yang. All authors reviewed the results and approved the final version of the manuscript.

REFERENCES

1. Papadoulis, A., M. Quddus, and M. Imprialou. Evaluating the Safety Impact of Connected and Autonomous Vehicles on Motorways. *Accident Analysis & Prevention*, Vol. 124, 2019, pp. 12–22. https://doi.org/10.1016/J.AAP.2018.12.019.

2. Kavas-Torris, O., S. Y. Gelbal, M. R. Cantas, B. Aksun Guvenc, and L. Guvenc. Connected UAV and CAV Coordination for Improved Road Network Safety and Mobility. *SAE Technical Papers*, No. 2021, 2021. https://doi.org/10.4271/2021-01-0173.

3. He, S., F. Ding, C. Lu, and Y. Qi. Impact of Connected and Autonomous Vehicle Dedicated Lane on the Freeway Traffic Efficiency. *European Transport Research Review*, Vol. 14, No. 1, 2022, pp. 1–14. https://doi.org/10.1186/S12544-022-00535-4/FIGURES/6.

4. Peng, B., M. F. Keskin, B. Kulcsár, and H. Wymeersch. Connected Autonomous Vehicles for Improving Mixed Traffic Efficiency in Unsignalized Intersections with Deep Reinforcement Learning. *Communications in Transportation Research*, Vol. 1, 2021, p. 100017. https://doi.org/10.1016/J.COMMTR.2021.100017.

5. Ge, J. I., and G. Orosz. Optimal Control of Connected Vehicle Systems With Communication Delay and Driver Reaction Time. *IEEE Transactions on Intelligent Transportation Systems*, Vol. 18, No. 8, 2017, pp. 2056–2070. https://doi.org/10.1109/TITS.2016.2633164.

6. Du, R., S. Chen, Y. Li, J. Dong, P. Y. J. Ha, and S. Labi. A Cooperative Control Framework for CAV Lane Change in a Mixed Traffic Environment. 2020.

7. Zhou, L., T. Ruan, K. Ma, C. Dong, and H. Wang. Impact of CAV Platoon Management on Traffic Flow Considering Degradation of Control Mode. *Physica A: Statistical Mechanics and its Applications*, Vol. 581, 2021, p. 126193. https://doi.org/10.1016/J.PHYSA.2021.126193.

8. Yang, H., and W. L. Jin. A Control Theoretic Formulation of Green Driving Strategies Based on Inter-Vehicle Communications. *Transportation Research Part C: Emerging Technologies*, Vol. 41, 2014, pp. 48–60. https://doi.org/10.1016/J.TRC.2014.01.016.

9. Hegyi, A., B. De Schutter, and H. Hellendoorn. Model Predictive Control for Optimal Coordination of Ramp Metering and Variable Speed Limits. *Transportation Research Part C: Emerging Technologies*, Vol. 13, No. 3, 2005, pp. 185–209. https://doi.org/10.1016/J.TRC.2004.08.001.

10. Chanut, S., and C. Buisson. Macroscopic Model and Its Numerical Solution for Two-Flow Mixed Traffic with Different Speeds and Lengths. *https://doi.org/10.3141/1852-26*, No. 1852, 2003, pp. 209–219. https://doi.org/10.3141/1852-26.

11. Bose, A., and P. A. Ioannou. Analysis of Traffic Flow with Mixed Manual and Semiautomated Vehicles. *IEEE Transactions on Intelligent Transportation Systems*, Vol. 4, No. 4, 2003, pp. 173–188. https://doi.org/10.1109/TITS.2003.821340.

12. Lo, S. C., and C. H. Hsu. Cellular Automata Simulation for Mixed Manual and Automated Control Traffic. *Mathematical and Computer Modelling*, Vol. 51, No. 7–8, 2010, pp. 1000–1007. https://doi.org/10.1016/J.MCM.2009.08.042.

13. Li, X., Y. Xiao, X. Zhao, X. Ma, and X. Wang. Modeling Mixed Traffic Flows of Human-Driving Vehicles and Connected and Autonomous Vehicles Considering Human Drivers' Cognitive Characteristics and Driving Behavior Interaction. *Physica A: Statistical Mechanics and its Applications*, Vol. 609, 2023, p. 128368. https://doi.org/10.1016/J.PHYSA.2022.128368.

14. Qin, Y., and H. Wang. Cell Transmission Model for Mixed Traffic Flow with Connected and Autonomous Vehicles. *Journal of Transportation Engineering, Part A: Systems*, Vol. 145, No. 5, 2019, p. 04019014. https://doi.org/10.1061/JTEPBS.0000238/ASSET/589EC17C-8E38-4CD2-B43D-1FCB1147D1DA/ASSETS/IMAGES/LARGE/FIGURE6.JPG.

15. Tajdari, F., and C. Roncoli. Adaptive Traffic Control at Motorway Bottlenecks with Time-Varying Fundamental Diagram. *IFAC-PapersOnLine*, Vol. 54, No. 2, 2021, pp. 271–277. https://doi.org/10.1016/J.IFACOL.2021.06.051.

16. Guo, Q., and X. (Jeff) J. Ban. Macroscopic Fundamental Diagram Based Perimeter Control Considering Dynamic User Equilibrium. *Transportation Research Part B: Methodological*, Vol. 136, 2020, pp. 87–109. https://doi.org/10.1016/J.TRB.2020.03.004.

17. Zhou, J., and F. Zhu. Modeling the Fundamental Diagram of Mixed Human-Driven and Connected Automated Vehicles. *Transportation Research Part C: Emerging Technologies*, Vol. 115, 2020, p. 102614. https://doi.org/10.1016/J.TRC.2020.102614.

18. Halakoo, M., and H. Yang. Evaluation of Macroscopic Fundamental Diagram Transition in the Era of Connected and Autonomous Vehicles. *IEEE Intelligent Vehicles Symposium, Proceedings*, Vol. 2021-July, 2021, pp. 1188–1193. https://doi.org/10.1109/IV48863.2021.9575687.

19. Shi, X., and X. Li. Constructing a Fundamental Diagram for Traffic Flow with Automated Vehicles: Methodology and Demonstration. *Transportation Research Part B: Methodological*, Vol. 150, 2021, pp. 279–292. https://doi.org/10.1016/J.TRB.2021.06.011.

20. Seraj, M., J. Li, and T. Z. Qiu. Expansion of the Fundamental Diagram from a Microscopic Multilane Modeling Framework of Mixed Traffic. 2020. https://doi.org/10.1155/2020/8878346.

21. Zhang, J., H. Pei, X. (Jeff) Ban, and L. Li. Analysis of Cooperative Driving Strategies at Road Network Level with Macroscopic Fundamental Diagram. *Transportation Research Part C: Emerging Technologies*, Vol. 135, 2022, p. 103503. https://doi.org/10.1016/J.TRC.2021.103503.

22. Treiber, M., and A. Kesting. *Traffic Flow Dynamics: Data, Models and Simulation*. Springer Berlin Heidelberg, 2013.

23. MESSNER, A., and M. PAPAGEORGIOU. METANET: A Macroscopic Simulation Program for Motorway Networks. *Traffic engineering & control*, Vol. 31, No. 8–9, 1990, pp. 466–470.